

Terahertz spectroscopic study of vertically aligned InN nanorods

H. Ahn, Y.-P. Ku, Y.-C. Wang, C.-H. Chuang, S. Gwo, and Ci-Ling Pan

Citation: *Applied Physics Letters* **91**, 163105 (2007); doi: 10.1063/1.2800292

View online: <http://dx.doi.org/10.1063/1.2800292>

View Table of Contents: <http://scitation.aip.org/content/aip/journal/apl/91/16?ver=pdfcov>

Published by the [AIP Publishing](#)

Articles you may be interested in

[N-type conductivity and properties of carbon-doped InN\(0001\) films grown by molecular beam epitaxy](#)

J. Appl. Phys. **113**, 033501 (2013); 10.1063/1.4775736

[Charge transport and trapping in InN nanowires investigated by scanning probe microscopy](#)

J. Appl. Phys. **106**, 124907 (2009); 10.1063/1.3273380

[Conductive atomic force microscopy study of InAs growth kinetics on vicinal GaAs \(110\)](#)

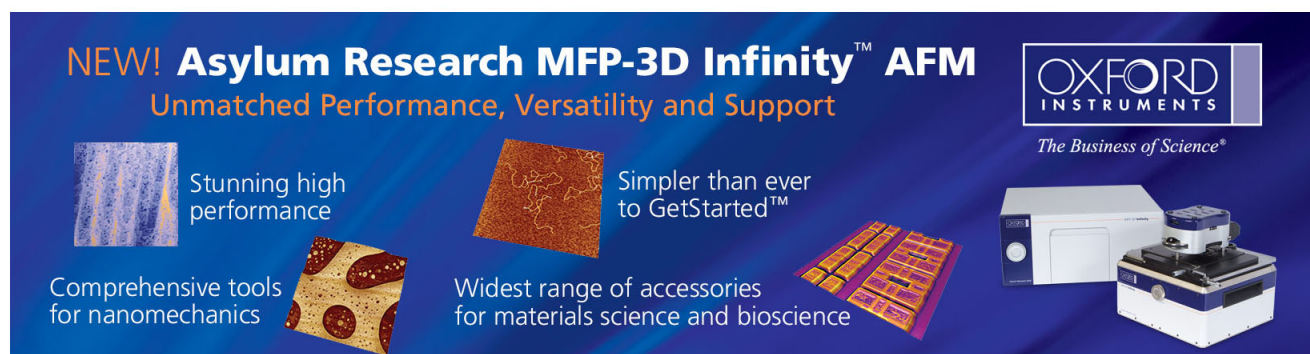
Appl. Phys. Lett. **95**, 123103 (2009); 10.1063/1.3232234

[Novelty and versatility of self-catalytic nanowire growth: A case study with InN nanowires](#)

J. Vac. Sci. Technol. B **25**, 940 (2007); 10.1116/1.2740275

[Electronic properties of InN nanowires](#)

Appl. Phys. Lett. **87**, 253103 (2005); 10.1063/1.2141927

The advertisement features a dark blue background with white and orange text. At the top left, it reads 'NEW! Asylum Research MFP-3D Infinity™ AFM' in large white letters, followed by 'Unmatched Performance, Versatility and Support' in orange. To the right is the Oxford Instruments logo, which includes the text 'OXFORD INSTRUMENTS' and the tagline 'The Business of Science®'. Below the main text are four images: a textured surface, a circular pattern, a grid of small squares, and the AFM instrument itself. Each image is accompanied by a short text description: 'Stunning high performance', 'Simpler than ever to GetStarted™', 'Comprehensive tools for nanomechanics', and 'Widest range of accessories for materials science and bioscience'.

Terahertz spectroscopic study of vertically aligned InN nanorods

H. Ahn,^{a)} Y.-P. Ku, Y.-C. Wang, and C.-H. Chuang

Department of Photonics and Institute of Electro-Optical Engineering, National Chiao Tung University, Hsinchu, 30010 Taiwan, Republic of China

S. Gwo

Department of Physics, National Tsing Hua University, Hsinchu, 30013 Taiwan, Republic of China

Ci-Ling Pan

Department of Photonics and Institute of Electro-Optical Engineering, National Chiao Tung University, Hsinchu, 30010 Taiwan, Republic of China

(Received 1 August 2007; accepted 27 September 2007; published online 16 October 2007)

Terahertz time-domain spectroscopy has been used to investigate terahertz conductivity and dielectric response of indium nitride (InN) nanorod array and epitaxial film. The complex terahertz conductivity of InN film is well fitted by the Drude model, while the negative imaginary conductivity of the InN nanorods can be described by using the Drude-Smith model. The electron mobility of the InN film is $1217 \pm 58 \text{ cm}^2/\text{V s}$, while that of the InN nanorods is $80 \pm 5 \text{ cm}^2/\text{V s}$. The reduced mobility of carriers for the latter can be attributed to the restricted carrier transport within the nanorods. © 2007 American Institute of Physics. [DOI: 10.1063/1.2800292]

Indium nitride (InN) is an interesting and potentially important semiconductor material with superior electronic transport properties over other group-III nitrides.¹ Recently, low-dimensional InN nanomaterials in the forms of nanowires, nanorods, nanotubes, etc., have received great attention due to their potential in near-infrared optoelectronics and photovoltaic applications. The discovery of the intrinsic narrow bandgap and remarkably large gap between the conduction band minimum and the next local minimum of InN also inspires potential applications in the terahertz range, for example, as an efficient terahertz emitter/detector.

To realize the prospect of terahertz applications, it is essential to understand fundamental terahertz properties of InN. To date, relatively few studies have explored InN and even fewer are reported for low-dimensional InN nanostructures. In this letter, we report the frequency-dependent complex terahertz conductivities and dielectric responses of the InN epilayer and vertically aligned InN nanorods measured by terahertz time-domain spectroscopy (TDS). Using the Drude model for carrier conduction, the key parameters that determine the free carrier dynamics of the InN film are extracted. Those parameters for the InN nanorods, however, are best fitted by applying a modified Drude model, which includes the scattering effect of electrons along the boundary of nanorods.

For this work, a wurtzite InN epitaxial film and vertically aligned InN nanorod array were grown on Si(111) substrates by plasma-assisted molecular beam epitaxy (PAMBE). To relax the heterointerface lattice mismatch, the InN epilayer was grown on Si(111) using the epitaxial AlN/ β -Si₃N₄ double-buffer layer technique and details of the growth procedure can be found elsewhere.² The InN nanorods were grown at 330 °C on β -Si₃N₄/Si(111) without the AlN buffer layer. Field-emission scanning electron microscopy (FE-SEM) images of the hexagonal shaped nanorods show that InN nanorods have a uniform diameter of

~130 nm with an average aspect ratio (height/diameter) of ~6 and have an aerial density of $\sim 5 \times 10^9 \text{ cm}^{-2}$. The thicknesses of the InN epilayer and nanorods are about 1.0 and 0.75 μm , respectively. The terahertz-TDS system is based on low-temperature-grown GaAs photoconductive dipole antennas excited and probed by a Ti:sapphire laser at a repetition rate of 82 MHz. Transmission of the terahertz signal is measured at normal incidence. The details of the apparatus has been described previously.³ The carrier density and mobility of the InN epitaxial film have been measured in separate room-temperature electron Hall measurements for comparison.

In terahertz-TDS analysis, measured time-domain terahertz waveforms from InN film, InN nanorods, and Si(111) substrates are Fourier transformed, and then the frequency-dependent dielectric constants of the InN samples are calculated from the spectral amplitude and phase difference between the samples and the substrate. Figure 1(a) shows the observed real (solid circles) and imaginary (open circles) parts of the frequency-dependent refractive index ($\tilde{n}=n+ik$) of the InN film. Both n and k decrease monotonically with increasing frequency. The complex dielectric constant is defined as $\varepsilon(\omega)=\varepsilon_{\infty}+i\sigma(\omega)/(\omega\varepsilon_0)=(n+ik)^2$, where ε_0 is the permittivity of free space, $\sigma(\omega)$ is the complex conductivity, and the dielectric constant ε_{∞} is 6.7 for InN.⁴ Using the above relationship for InN, we find the real part of conductivity, $\text{Re}[\sigma]$ decreases as the frequency increases, while $\text{Im}[\sigma]$ increases slowly [see Fig. 1(b)]. This frequency dependence is typically observed for Drude-like materials below the plasma frequency. We, thus, fit the measured complex refractive index and conductivity in Fig. 1 using the simple Drude model,⁵ in which the complex conductivity is defined by $\sigma(\omega)=\varepsilon_0\omega_p^2\tau_0/(1-i\omega\tau_0)$; $\omega_p^2=Ne^2/(m^*\varepsilon_0)$ is the plasma frequency and τ_0 is the carrier scattering time. For the InN film, it was determined that $\omega_p/2\pi=52 \pm 1.2 \text{ THz}$ and $\tau_0=52 \pm 2.5 \text{ fs}$. Assuming an electron effective mass $m^*=0.075m_0$ for the InN film,⁴ these fitting parameters correspond to a carrier density $N=\omega_p^2m^*\varepsilon_0/e^2=2.5 \pm 0.2 \times 10^{18} \text{ cm}^{-3}$ and a carrier mobility $\mu=e\tau_0/m^*$

^{a)} Author to whom correspondence should be addressed. Electronic mail: hyahn@mail.nctu.edu.tw

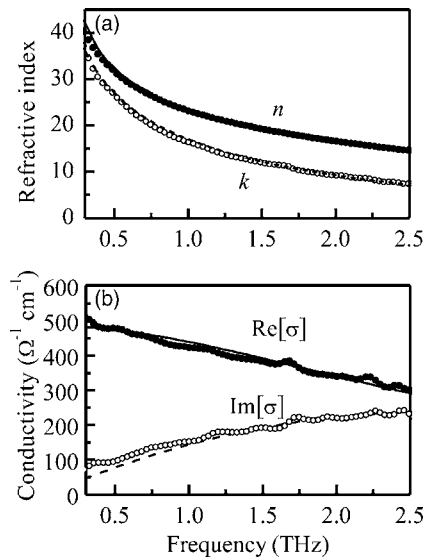


FIG. 1. Real (solid circles) and imaginary (open circles) parts of (a) refractive index and (b) conductivity of the InN film. Solid and dashed lines correspond to the calculated results based on the simple-Drude model. The fitting parameters are listed in Table I.

$=1217 \pm 58 \text{ cm}^2/\text{V s}$. These values are in reasonable agreement with room-temperature Hall effect measurement results of $3.1 \times 10^{18} \text{ cm}^{-3}$ and $1036 \text{ cm}^2/\text{V s}$, respectively. The fitting parameters are listed in Table I.

Since the InN nanorod film is consisted of loosely packed InN nanorods and air, the physical parameters directly measured from the data of time-domain terahertz waveforms contain the contributions from both the air and the pure InN nanorods. To obtain the physical parameters of the pure InN nanorods, a simple effective medium approximation (EMA),⁶ $\epsilon_{\text{eff}}(\omega) = f\epsilon_m(\omega) + (1-f)\epsilon_h$, was employed, where the filling factor $f \sim 0.7$ is obtained from the SEM image shown as an inset in Fig. 2(a), and $\epsilon_m(\omega)$ and ϵ_h are the dielectric constants of the pure InN nanorods and the host medium (air) respectively. Figures 2(a) and 2(b) illustrate frequency-dependent refractive index and conductivity of the pure InN nanorods extracted under EMA, respectively. The trend of monotonic decrease of the complex refractive index of the nanorods is similar to the case of InN film. The complex conductivity response of the nanorods, however, is different from that of InN film. $\text{Re}[\sigma]$ gradually increases with increasing frequency, while $\text{Im}[\sigma]$ with a negative value decreases with increasing frequency. This frequency dependence cannot be explained by the simple Drude model, in which the frequency-dependent conductivity has a maximum at zero frequency and monotonically decreases with frequency. Recently, Smith proposed a modified Drude model (Drude-Smith model),⁷ which has been used in the interpretation of the negative $\text{Im}[\sigma]$ observed in nanostructures.^{8,9}

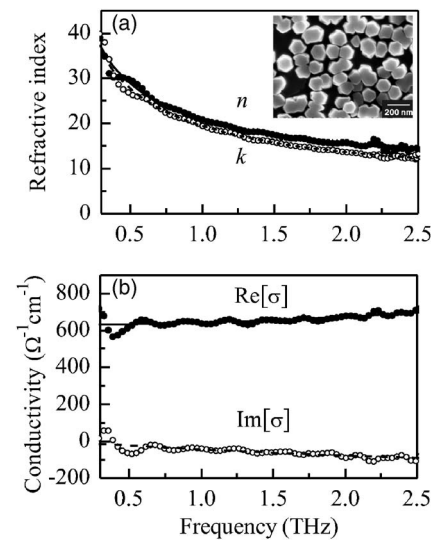


FIG. 2. Real (solid circles) and imaginary (open circles) parts of (a) refractive index and (b) conductivity of the InN nanorods. Solid and dashed lines correspond to the calculated results based on the Drude-Smith model. Inset: FE-SEM image of the InN nanorods in the plan view.

The complex conductivity in the Drude-Smith model is given by⁷

$$\sigma(\omega) = \frac{Ne^2\tau_0/m^*}{1 - i\omega\tau_0} \left[1 + \sum_j \frac{c_j}{(1 - i\omega\tau_0)^j} \right],$$

where c_j is a parameter describing fraction of the electron's original velocity after some number j of scattering events. In practice, we take only the first term in c_j [$c_1 = c$] and then c varies between -1 and 0 , corresponding to Drude conductivity for $c=0$ and complete backscattering for $c=-1$.

Using the Drude-Smith model, an excellent fit of complex conductivity of the InN nanorods is obtained with the fit parameters $c = -0.65 \pm 0.01$, $\tau_0 = 13 \pm 0.2 \text{ fs}$, and $\omega_p/2\pi = 199 \pm 3 \text{ THz}$. These are shown in Fig. 2. Here, a large negative value of $c = -0.65$ for InN nanorods reflects that the localized electrons may experience a preferential backward scattering due to electron scattering from defects in InN nanorods caused by the increased structural disorders¹⁰ or a Coulombic restoring force from charged defects.¹¹ In the Drude-Smith model, the electron mobility is given by $\mu_m = (1+c)(e\tau_0/m^*)$, which requires the exact value of the effective mass m^* of the InN nanorods. However, up to now no reasonable value of m^* of the pure InN nanorod is available in the literature. Recently, we have shown that vertically aligned InN nanorod arrays grown on silicon by PAMBE possess the crystal properties similar to wurtzite InN single crystal.^{10,12} Therefore, we assume that N versus m^* relation of the InN nanorods follows that of InN single crystal. From previously measured near-infrared photoluminescence

TABLE I. Extracted parameters for best fits in Figs. 1 (InN film) and 2 (InN nanorods) compared to those obtained from dc Hall measurements and room-temperature Raman measurement.

Sample	Thickness (nm)	Fitted Carrier concentration ($\times 10^{19} \text{ cm}^{-3}$)	Fitted mobility ($\text{cm}^2/\text{V s}$)	Carrier concentration ($\times 10^{19} \text{ cm}^{-3}$)	Hall mobility ($\text{cm}^2/\text{V s}$)
InN film	1000	0.25 ± 0.02	1217 ± 58	0.31	1036
InN nanorods	750	4.9 ± 0.2	80 ± 5	1.5^a	N.A.

^aReference 12.

and room-temperature polarized-Raman scattering data,¹² the carrier density of the InN nanorods is predicted to be $\sim 1.5 \times 10^{19} \text{ cm}^{-3}$. The corresponding effective mass of $0.10m_0$ is then estimated from the N versus m^* relation calculated by Kane's two-band $\mathbf{k} \cdot \mathbf{p}$ model combined with band normalization effect.¹³ Using this estimated m^* and the best fit parameters to the Drude-Smith model, an electron mobility of $80 \pm 5 \text{ cm}^2/\text{V s}$ with an electron density of $4.9 \pm 0.2 \times 10^{19} \text{ cm}^{-3}$ is obtained for the InN nanorod array. High carrier density and large effective mass of the InN nanorods are ascribed to structural defects, which push the Fermi energy high in the conduction band¹⁴ and the conduction band nonparabolicity due to the $\mathbf{k} \cdot \mathbf{p}$ interaction across the narrow direct gap between the conduction band and valence band in InN.¹⁵

The reduced dc conductivity in the Drude-Smith model is given by $\sigma(\omega=0) = (1+c)(eN\mu)$. Therefore, a large negative value of c implies that electron backscattering occurs at the boundaries and surfaces of nanostructures and consequently suppresses dc conductivity. The value of $c = -0.65$ obtained for InN nanorods reflects that the degree of backscattering of electrons increases due to the confinement of carriers inside a cylindrical nanorod. Despite the InN nanorods are vertically well aligned, they are quite disordered in lateral alignment. The separation between the InN nanorods can be of the order of the nanorod lateral size [see the inset in Fig. 2(a)]. Therefore, inter-rod transport due to the electronic coupling between isolated nanorods may be prohibited. Consequently, the observed reduce mobility of the InN nanorods could be attributed to the intra-rod transport of electrons within the nanorods.

To be more quantitative, we calculate the electron mean free path (MFP) at room temperature ($T \sim 300 \text{ K}$). Given a thermal velocity of $\sim 1.2 \times 10^5 \text{ m/s}$, the measured scattering time of 13 fs for the InN nanorods results in the MFP of $\sim 2 \text{ nm}$, which is much smaller than the average nanorod radius of 65 nm. We, thus, expect that carriers would undergo Drude-like scattering ($c=0$) as well as backscattering ($c=-1$) within the nanorods. This can be understood from the value of $c = -0.65$, which is considerably larger than that of small size (of the order of nm) nanostructures with $c \approx -1$.^{8,9}

In summary, we have investigated physical parameters of the InN film and the InN nanorods using terahertz-TDS. The complex terahertz conductivity of InN film is well fitted by the Drude model, while the negative imaginary conductivity of InN nanorods can be described by using the Drude-Smith model. The electron mobility of the InN film is $1217 \pm 58 \text{ cm}^2/\text{V s}$, while that of the InN nanorods is $80 \pm 5 \text{ cm}^2/\text{V s}$. The drastically reduced electric mobility of the InN nanorods compared to that of the InN film is due to the suppressed inter-rod transport of electrons.

This work was supported in part by the National Science Council (NSC) through several grants including NSC 96-2112-M-009-016-MY3, PPAEU-II, and the ATU program of the Ministry of Education, Taiwan.

¹A. G. Bhuiyan, A. Hashimoto, and A. Yamamoto, *J. Appl. Phys.* **94**, 2779 (2003), and references therein.

²S. Gwo, C.-L. Wu, C.-H. Shen, W.-H. Chang, T. M. Hsu, J.-S. Wang, and J.-T. Hsu, *Appl. Phys. Lett.* **84**, 3765 (2004).

³C.-L. Pan, C.-F. Hsieh, R.-P. Pan, M. Tanaka, F. Miyamaru, M. Tani, and M. Hangyo, *Opt. Express* **13**, 3921 (2005).

⁴A. Kasic, M. Schubert, Y. Satio, Y. Nanishi, and G. Wagner, *Phys. Rev. B* **65**, 115206 (2002).

⁵T.-I. Jeon and D. Grischkowsky, *Phys. Rev. Lett.* **78**, 1106 (1997).

⁶F. J. Garcia-Vidal, J. M. Pitarke, and J. B. Pendry, *Phys. Rev. Lett.* **78**, 4289 (1997); H.-Ch. Weissker, J. Furthmuller, and F. Bechstedt, *Phys. Rev. B* **67**, 165322 (2003).

⁷N. V. Smith, *Phys. Rev. B* **64**, 155106 (2001).

⁸D. G. Cooke, A. N. MacDonald, A. Hryciw, J. Wang, Q. Li, A. Meldrum, and F. A. Hegmann, *Phys. Rev. B* **73**, 193311 (2006).

⁹G. M. Turner, M. C. Beard, and C. A. Schmuttenmaer, *J. Phys. Chem. B* **106**, 11716 (2002); M. Beard, G. M. Turner, J. E. Murphy, O. I. Micic, M. C. Hanna, A. J. Nozik, and C. A. Schmuttenmaer, *Nano Lett.* **3**, 1695 (2003).

¹⁰C.-H. Shen, H.-Y. Chen, H.-W. Lin, S. Gwo, A. A. Klochikhin, and V. Yu. Davydov, *Appl. Phys. Lett.* **88**, 253104 (2006).

¹¹J. B. Baxter and C. A. Schmuttenmaer, *J. Phys. Chem. B* **110**, 25229 (2006).

¹²H.-Y. Chen, C.-H. Shen, H.-W. Lin, C.-H. Chen, C.-Y. Wu, S. Gwo, A. A. Klochikhin, and V. Yu. Davydov, *Thin Solid Films* **515**, 961 (2006).

¹³S. P. Fu and Y. F. Chen, *Appl. Phys. Lett.* **85**, 1523 (2004).

¹⁴S. X. Li, K. M. Yu, J. Wu, R. E. Jones, W. Walukiewicz, J. W. Ager III, W. Shan, E. E. Haller, Hai Lu, and William J. Schaff, *Phys. Rev. B* **71**, 161201 (2005).

¹⁵H. A. Washburn, J. R. Sites, and H. H. Wieder, *J. Appl. Phys.* **50**, 4872 (1979).